2022 IEEE Applied Power Electronics Conference and Exposition (APEC), Houston, TX, USA, March 2022

A Bidirectional Liquid-Cooled GaN-based AC/DC Flying Capacitor Multi-Level Converter with Integrated Startup and Additively Manufactured Cold-Plate for Electric Vehicle Charging

K. Fernandez
R. Iyer
T. Ge
J. Zou
D. Chou
Z. Liao
V. Agarwal
T. Gebrael
N. Miljkovic
R. C. N. Pilawa-Podgurski

A Bidirectional Liquid-Cooled GaN-based AC/DC Flying Capacitor Multi-Level Converter with Integrated Startup and Additively Manufactured Cold-Plate for Electric Vehicle Charging

Kelly Fernandez*, Rahul Iyer*, Ting Ge*, Jiarui Zou*, Derek Chou*, Zitao Liao*, Vaibhav Agarwal†, Tarek Gebrael†
Nenad Miljkovic†, Robert C.N. Pilawa-Podgurski*
email: kefernandez@berkeley.edu, rkiyer@berkeley.edu
* University of California, Berkeley. Berkeley, CA 94720 USA
† University of Illinois at Urbana-Champaign. Urbana, IL, 61801 USA

***Abstract*—Level II electric vehicle (EV) on-board chargers provide AC-DC conversion capability in order to charge on-board high-voltage (HV) batteries. Bidirectional EV chargers can allow the EV to also act as an AC source in vehicle-to-grid services. In both charging and inverter applications, it is desirable for chargers to have high power density, high power-handling capability, and low weight. This paper showcases the architecture and control of an optimized bidirectional EV charger system that can convert from both low-line (120 V_{AC}) and high-line (240 V_{AC}) AC voltages to a 400 V_{DC} output. The operation and control of the complete system, thermal management, enhanced power stage design, and start-up procedure are discussed. Experimental results demonstrating DC-AC high power operation and system start-up are reported.**

I. Introduction

Level II on-board electric vehicle (EV) chargers interface with the AC grid in order to charge the high-voltage battery inside the EV and may also provide energy back to the grid for vehicle-to-grid services. As a result, EV chargers are required to handle a variety of AC grid voltages (120-240 V_{AC}) at power levels in the kilowatt range [1]. EV chargers need to have high power-handling capability and high efficiency in order to provide faster charging times that compete with the refueling times of gasoline powered vehicles [2], [3]. Moreover, it is advantageous for on-board chargers to demonstrate low volume and weight due to their location inside the vehicle at all times.

Previous work has shown that a modular single-phase converter design consisting of a flying capacitor multilevel (FCML) power stage and a series-stacked buffer (SSB) for twice-line-frequency energy buffering can demonstrate high power density and high efficiency compared to conventional solutions consisting of two-level converters and electrolytic capacitors for energy buffering [4], [5]. A system schematic for the combined FCML and SSB EV charger solution is depicted in Fig. 1.

In this work, power converter design, thermal optimization and integration, and a novel converter start-up procedure are discussed. The FCML converters are designed for heavy-load operation and low parasitic inductance, enabling sharper switching transitions afforded by Gallium Nitride (GaN) power switches. A custom additively manufactured cold-plate interfaces with the power switches and inductors and features improved internal coolant channels to enable more effective heat transfer. The optimized coolant loop design and additive manufacturing enable improvement of the gravimetric and volumetric power density of the overall system. An active start-up circuit and accompanying control procedure are demonstrated for the first time in such a system, and enable soft-starting the FCML from a grid connection while ensuring flying capacitor voltage balancing and minimizing switch stresses. Test results demonstrating steady-state DC-AC inverter operation from 400 V_{DC} to 240 V_{AC} RMS at kilowatt levels, and transient start-up AC-DC operation from 120 V_{AC} RMS to 400 V_{DC} are provided.

II. System Architecture

The EV charger electrical system schematic is shown in Fig. 1. From the AC to the DC port, the electrical system consists of a full-bridge stage that rectifies the AC input, two interleaved FCML converters that function as the power factor correction (PFC) boost stage, and an SSB module that buffers the twice-line frequency power pulsation on the DC bus. The system's controller designs are detailed in [5].

A. FCML Stage

The FCML stage, as shown in Fig. 1, is comprised of two interleaved bidirectional FCML converters, and can be controlled to act either as a PFC rectifier or as an inverter. When the system is controlled for PFC rectification, the FCML stage operates in a boost mode, and the inductor current is regulated to be in phase with the AC input voltage. When the system is controlled as an inverter, the FCML stage operates in a buck mode, and produces a rectified sine wave. In both cases, a cascaded full-bridge stage comprised of high-conductivity

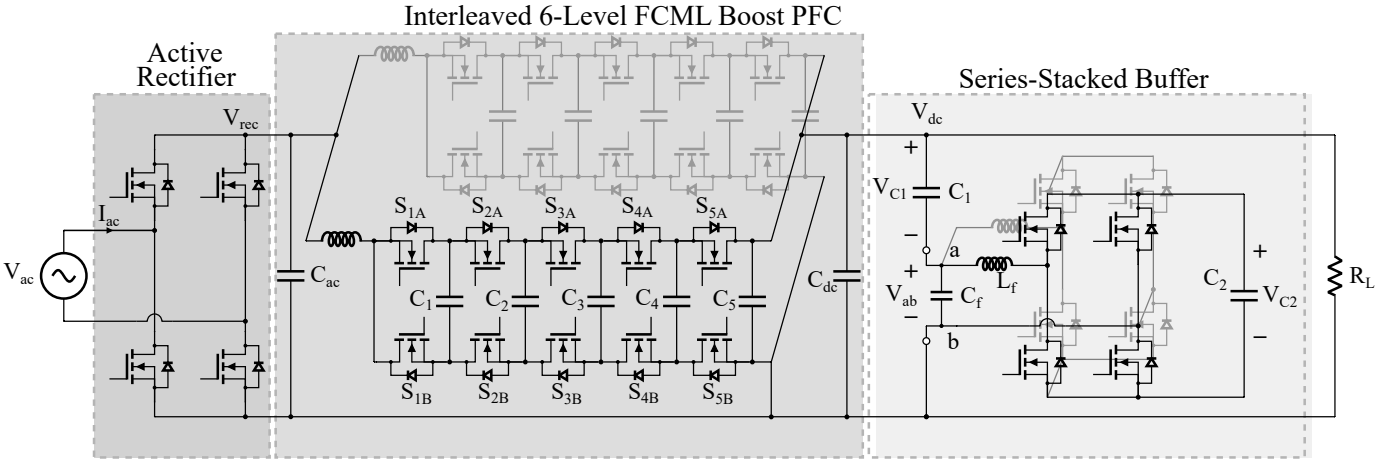

Fig. 1: Schematic of the overall system with active rectifier (unfolder), interleaved FCML PFC, and series-stacked buffer.

devices acts as an active rectifier and interfaces the LC filter of the FCML converter to the grid voltage [4].

B. Series-Stacked-Buffer Stage

The SSB architecture and control for charging applications are detailed in [6], [7]. Capacitor C_1 is the main energy-buffering capacitor and is connected in series with a full-bridge converter. Capacitor C_2 operates as the DC voltage source for the full-bridge converter. Voltage v_{C1} is allowed to have large AC voltage ripple, which is cancelled by the voltage produced by the full-bridge converter v_{ab}. The derivation of voltage v_{ab} can be found in [7]. Because v_{C1} is allowed to have large ripple, the capacitance and volume of C_1 can be greatly reduced compared to conventional DC bus capacitor filters. Moreover, because the DC bus voltage is displaced across C_1, a minimal real power is processed by the full-bridge, allowing for further improvements in the overall system efficiency.

C. Start-Up

Before the system can begin charging the EV battery from the AC grid, the flying capacitors of the FCML converters must be charged up to their respective nominal voltages. Even if the FCML converter's power switches are able to tolerate high surge currents, voltage sources cannot be instantaneously connected to either port because the power switches are typically not rated for the full DC bus voltage. To illustrate this point, Fig. 2 shows an N-level FCML in this hard-start-up scenario. In this depiction, V_{high} represents the voltage on the DC port of the EV charger system, while V_{low} is the voltage induced on the rectified node of the AC port. We assume the converter is initially disconnected from the DC battery and is instantaneously connected to the rectified grid voltage at its AC port. Furthermore, we assume that after the instantaneous connection of the AC source, a positive voltage is applied to the AC port of the system, enabling V_{low} to rise above 0 V. Typically, V_{high} is initially disconnected from the battery, using a mechanical or a solid-state relay, rendering the V_{high} terminal floating, and the high-side switches conduct through their reverse-conduction mechanism. The voltage V_{high} is then approximately

$$V_{high} \approx V_{low} - (N-1) \cdot V_r, \tag{1}$$

where V_r is the reverse conduction voltage of the FCML semiconductor switches and N is the number of levels of the FCML (N = 6 for this system). The voltage across switches $S_{(N-1)A}$ and $S_{(N-1)B}$ are approximately

$$V_{S(N-1)A} \approx -V_r, \tag{2}$$

and

$$V_{S(N-1)B} \approx V_{low} - (N-2) \cdot V_r. \tag{3}$$

Switch $S_{(N-1)B}$ is typically designed to block a nominal voltage of $V_{dc}/(N-1)$. Compared to this nominal blocking voltage, the instantaneous voltage given in (3) can be greater, as V_{low} can be as high as the peak line voltage. Therefore, for typical FCML designs, the converter terminal voltages cannot be applied instantaneously. Prior literature has explored "soft-starting" the FCML converters by slowly ramping the terminal voltages through passive means [8], or in the case

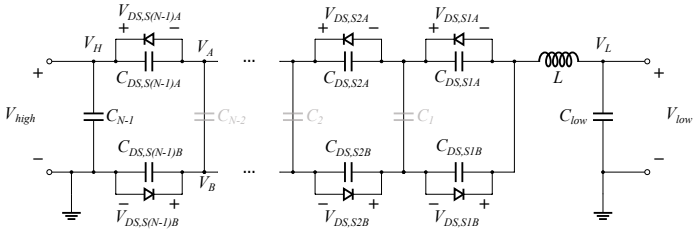

Fig. 2: Schematic model of an N-level FCML converter during a hard start-up where AC-side voltage source is applied to the converter instantaneously. The flying capacitors shown appear as virtual shorts instantly after the voltage is applied. We assume low inductance and large flying capacitance as is typical.

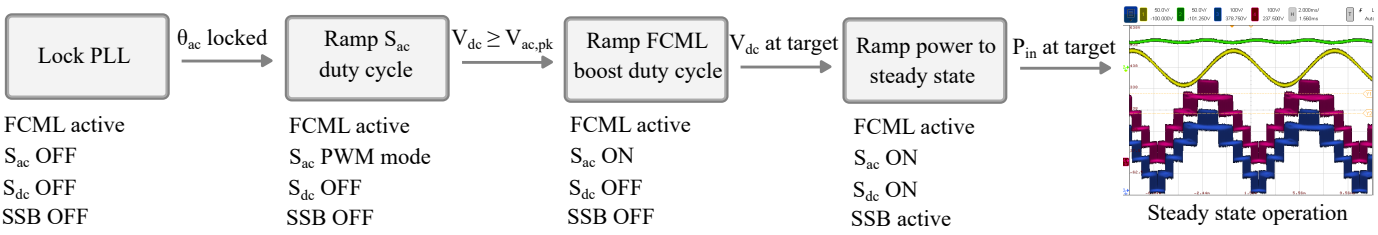

Fig. 3: Flow diagram of the EV charger start-up control procedure.

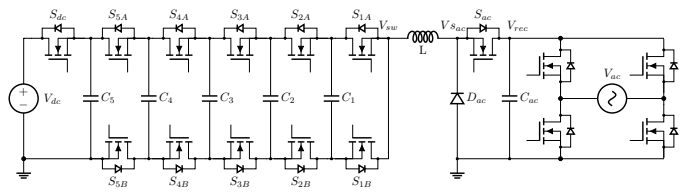

Fig. 4: Schematic of EV charger FCML equipped with start-up components S_{ac} and D_{ac}.

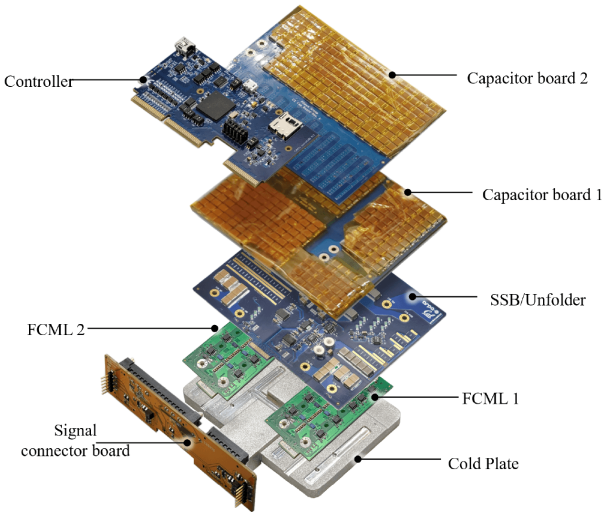

Fig. 5: Breakdown of the charger assembly, showing the modular hardware design. The FCMLs designed in this work interface to the custom additively manufactured cold-plate.

of the DC-AC converter of [9], a modulation technique is provided that manages a defined fast-ramping input voltage. In this work, an active start-up circuit and corresponding control are proposed, enabling a compact solution for converter start-up. The schematic drawing of a FCML converter equipped with the proposed start-up hardware is shown in Fig. 4. The start-up components consist of switch S_{ac} and diode D_{ac} on the AC side, and switch S_{dc} on the DC side.

Figure 3 displays the proposed start-up control diagram. First, the phase-locked loop (PLL) determines the phase angle of the input AC voltage. This enables the controller to synchronize the rectifier switching with the grid voltage zero-crossings, and provides instantaneous AC-side voltage information to the start-up controller. Next, the duty ratio for S_{ac} is ramped from 0 to 1, where S_{ac} is operated in pulse-width modulation (PWM) mode. In this interval, the average value of $V_{S_{ac}}$ lies below the grid voltage amplitude. The DC-side voltage V_{dc} rises simultaneously via control of the FCML switches to match the rectified AC amplitude at $V_{S_{ac}}$. When the duty ratio for S_{ac} reaches its final value of 1, the FCML stage regulates its DC-side voltage to track a ramped reference value. The DC voltage ramp terminates at the desired DC bus voltage, at which point S_{dc} can be turned on to connect the DC battery to the FCML converter. The EV charger now acts as a boost PFC and can be commanded to supply the DC battery with the requisite power.

III. Hardware Implementation

Figure 5 shows the constructed hardware prototype of the proposed system and control. Table I lists the hardware components used in the sub-modules of the EV charger system. The hardware prototype is comprised of two interleaved FCML converters, an SSB with energy storage capacitor C_1 and full-bridge DC source capacitor C_2, a full-bridge active rectifier, and a logic connector board. The logic connector board connects to the FCMLs, SSB, and active rectifier stages to a TI C2000 microcontroller (TMS320F28379D) on which the system control loops are implemented. Power is transferred from one module to another via bolt-type connectors. The design philosophy of the 3D integration for both the electrical and thermal systems is discussed in [5]. The start-up module is shown in Fig. 8. It is connected to the system between the active rectifier bridge and the FCML filter inductor.

A. FCML Module

The FCML module is designed to handle high output currents while tolerating flying capacitor imbalance. The maximum DC voltage of each FCML module is 400 V. Therefore, each switch will have to nominally block 80 V [4]. Under heavy load or transient conditions, the flying capacitor voltages may experience voltage imbalance [10], causing the blocking voltages of the switches to also increase past the nominal value. To resolve this issue, switches with a higher voltage rating can be implemented in the FCML module. Specifically, a high voltage power semiconductor can be chosen that has low $R_{DS,on}$, which further enables lower conduction loss and higher efficiency at high power operation. Our strategy of increasing the device voltage rating to handle higher load current instead of increasing the flying capacitance allows us to increase our passive component energy utilization and

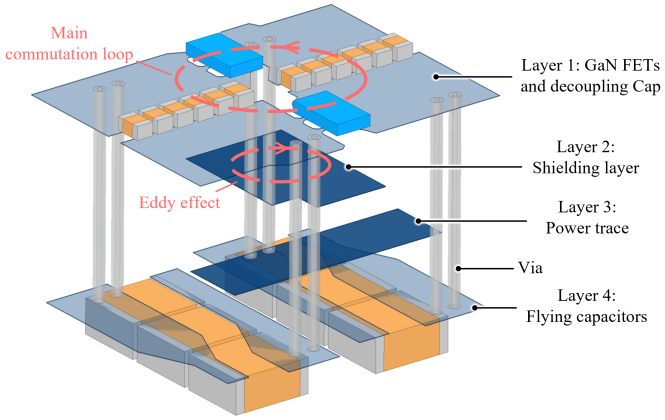

Fig. 6: PCB design of FCML module power stage that uses copper shield planes to reduce the parasitic loop inductance.

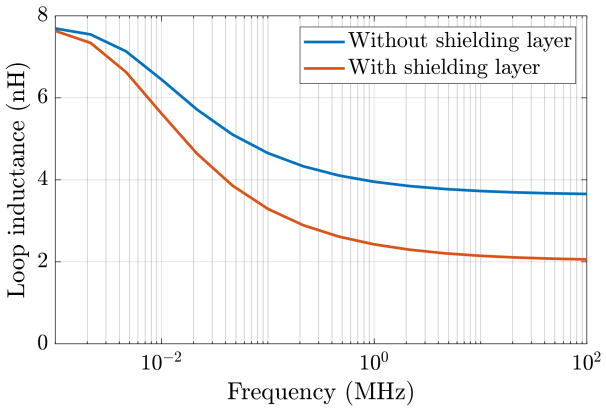

Fig. 7: Commutation loop inductance simulated in ANSYS Q3D for lateral commutation loop with and without shielding layer.

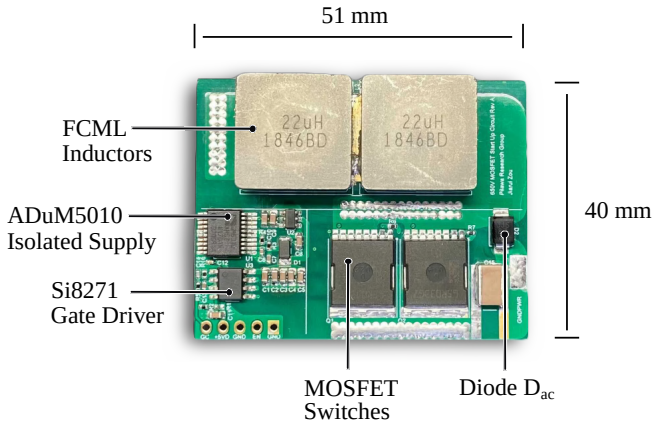

Fig. 8: Modular start-up PCB daughter-board that is fitted to the EV charger system.

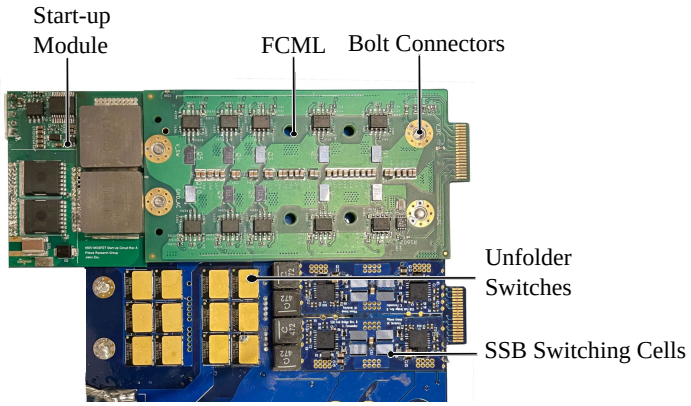

Fig. 9: Start-up PCB daughter-board shown mounted next to the FCML converter PCB. The charger's modular design simplifies assembly and enables dense system integration.

prevent power density penalties associated with larger flying capacitance at high power operation.

The parasitic inductance associated with the switching commutation loops in the FCML converter was studied and decreased via the insertion of inner shielding layers in the printed circuit board. Commutation loop inductance is critical to high-performance converter design, as it directly impacts switch voltage stress as a result of ringing at the switching edges [11]. In this work, copper shield planes [11], [12] were placed directly under each commutation loop consisting of a complementary switch pair and adjacent flying capacitors. The benefits of the copper shielding layer can be visualized through the effects of eddy currents. Figure 6 shows the location of the copper shield planes and the eddy current induced from the power stage current. The current transient in the power stage creates a changing magnetic field, which induces eddy currents inside the shield plane. As a result of this magnetic field cancellation, the loop inductance and the drain-to-source voltage ringing associated with each switch transition are greatly reduced. Fig. 7 shows the loop inductance of the FCML modules simulated in ANSYS Q3D with and without a copper shielding layer. With the addition of a copper shield plane, the commutation loop inductance decreases and is nearly halved at higher frequencies.

B. Start-Up Module

A start-up circuit daughter-board shown in Fig. 8 is designed to integrate the startup devices S_{ac} and D_{ac} and associated gate-drive hardware. The start-up module interfaces the active rectifier and the FCML converter's filter inductor. A PWM control signal from the microcontroller is fed to the gate-driver IC. Since the source of S_{ac} floats above the system ground potential, an isolated supply is needed to deliver gate drive power. Four 650 V Silicon MOSFETs, two on each side of the module, are connected in parallel to increase the current handling capability of the series device S_{ac}. The daughter-board is shown assembled with the FCML converter in Fig. 9. Both PCBs are mounted on a carrier board also containing the SSB and active rectifier.

TABLE I: Component listing

Subsystem	Component	Part No.	Parameters
Interleaved 6-Level FCML (per leg)	GaN FETs	EPC2033	150 V, 7 $m\Omega$
	Isolated Gate Drivers	Si8271GB-IS	Silicon Labs Si827x Series
	Flying Capacitors	TDK C5750X6S225K250KA	2.2 μF $\times$ 2–5 (parallel, $\sim$ 2.6μF effective)
	Inductors	Vishay IHLP6767GZER100M11	10 μH
Active Rectifier / Unfolder	GaN FETs	GaN Systems GS66516T	650 V, 25 $m\Omega\times$ 3 (parallel)
	Isolated Gate Drivers	Si8274GB1-IS1	Silicon Labs Si827x Series
Interleaved Series-Stacked Buffer (per leg)	GaN FETs	EPC 2033	150 V, 7 $m\Omega$
	Isolated Gate Drivers	Si8274GB1-IM1	Silicon Labs Si827x Series
	Inductors	Coilcraft XAL7070-472	4.7 μH $\times$ 2 (series)
Buffer Capacitors	C_1	TDK C5750X6S225K250KA	$\times$ 820 (parallel)
	C_2	TDK C5750X7S2A156M250KB	$\times$ 200 (parallel)
Control	Microcontroller	TI F28379D controlCARD	C2000 Series Microcontroller
Start-Up	MOSFETs	Infineon IPT65R033G7	650 V, 33 $m\Omega$ x 4 (parallel)
	Diode	ON Semiconductor MUR160G	600 V, 1 A
	Isolated Gate Driver	Si8271GB-IS	Silicon Labs Si827x Series
	Isolated Gate Driver	ADuM5010	Analog Devices isoPower

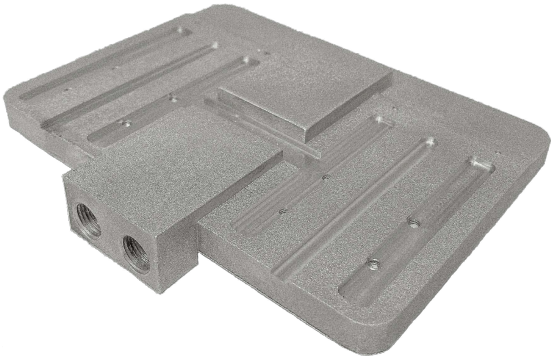

Fig. 10: Custom additively manufactured cold-plate, showing the side which interfaces with the electrical system.

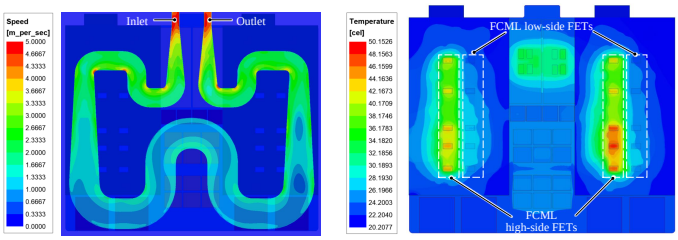

Fig. 11: Simulated velocity magnitude of the coolant with a 3.3 LPM flow and corresponding temperature on the power stage operating at 4 kW.

C. Cold-Plate

Figure 10 shows the custom additively manufactured cold-plate that was used to liquid-cool the EV charger electrical system. The cold-plate used in this work incorporates a highly optimized fluid flow path to ensure efficient heat removal from the converter assembly. The pressure drop across the cold-plate and its mass were considered as optimization objectives in the design optimization process. An aluminum silicon (AlSi10Mg) direct metal laser sintering (DMLS) additive manufacturing process was chosen for the cold-plate construction to enable complex internal geometries needed for fluid flow and weight reduction. Additive manufacturing permits the design of a curved fluid flow path with a non-circular channel cross-section. This enables increased heat exchange between the inner fluid and the cold-plate surface, and significantly reduces loss of fluid pressure over the fluid path length. The custom additively manufactured cold-plate design has an approximate differential pressure drop of 4 PSI. The cold-plate weighs approximately 240 grams and occupies a total volume of 7 cm^3.

The velocity of the coolant fluid (water in this design) and the estimated temperatures of the power switches and inductors on the charger PCBs are simulated in ANSYS IcePAK. The simulation results are shown in Fig. 11. Power switch and inductor losses are estimated based on LTspice simulation of the FCML converters in buck mode, representing the system operating as an inverter. Manufacturer GaN SPICE models are used for improved modeling of switching and conduction losses. The simulation reveals that the high-side switches in the FCML converters demonstrate higher loss compared to their low-side counterparts due to their hard-switching operation, and thus have higher temperature. The difference in temperature between the low-side and high-side devices is highlighted in Fig. 11. The left-side FCML converter demonstrates a relatively lower temperature than the right-side one since the high-side FETs of the left-side FCML converter are closer to the fluid flow pipeline. This matches the findings in [5].

IV. Experimental Results

The EV charger system was tested up to 3.8 kW operating as an inverter. The electrical system was connected to a 400 V$_{DC}$ input source, producing a 240 V AC RMS output. Figure 13 shows the electrical system efficiency over a 500 W to 3.8 kW power range. The system's efficiency and corresponding power

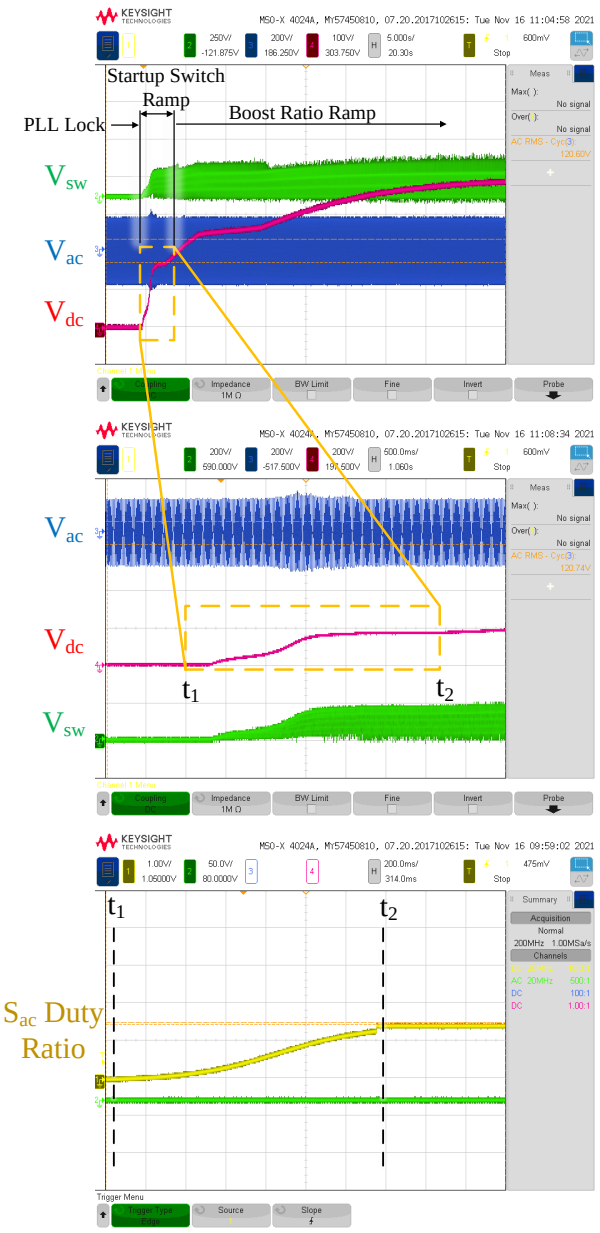

Fig. 12: Annotated start-up waveforms showing start-up switch ramp phase, and corresponding start-up switch duty ratio ramp.

is 98.5% at 1.7 kW while the efficiency at max power is 97.4%. The efficiency and power measurements were taken with the Keysight PA2201 power analyzer. Figure 14 displays the FCML converters' switched node voltage waveforms, which exhibit stable balanced operation. Figure 14 also shows the key SSB voltage waveforms that demonstrate twice-line-frequency energy buffering on the DC bus.

To test the proposed start-up circuit, the system is connected to an AC supply with the start-up procedure enabled. Key waveforms during converter start-up with annotations highlighting the different phases of the start-up control are shown in Fig. 12. The system was connected to a 120 V_{AC} source

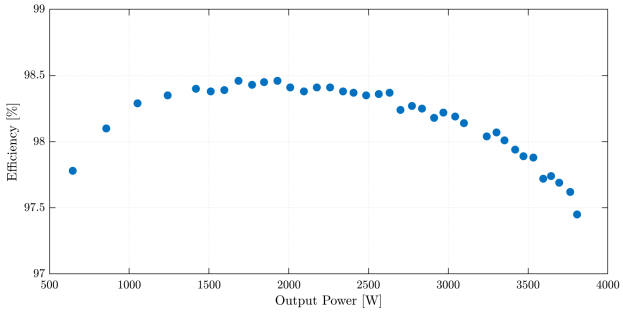

Fig. 13: The efficiency of the system in inverter mode from 400 V_{DC} to 240 V_{AC}.

https://www.overleaf.com/project/619552d885b14c032f4da691

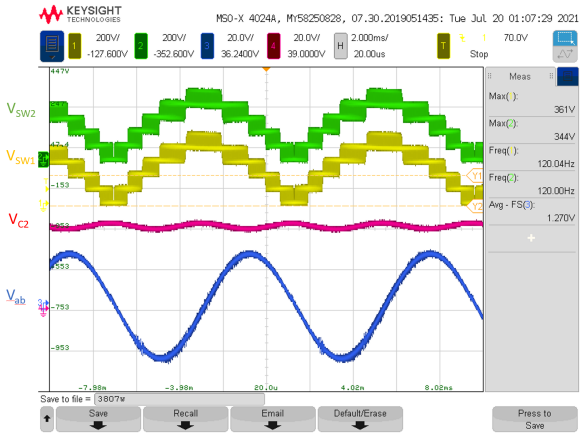

Fig. 14: FCML switching waveforms measured at peak tested power (3.8 kW). The measured switched-node waveforms indicate natural balancing of the flying capacitor voltages.

and commanded a target DC output of 400 V_{DC}. The start-up control and hardware allow for the DC-side voltage V_{DC} to be ramped from 0 V to 400 V in a safe manner.

V. Conclusions

In this paper, we investigate a bidirectional EV charging system consisting of FCML and SSB stages. Improvements in the converter's design and component selection and an optimized additively manufactured cold-plate enable demonstration of a compact and lightweight prototype. The system is tested up to 3.8 kW. We also demonstrate reliable converter start-up from an AC source using a novel soft-start sequence for charging the flying capacitors. The start-up hardware and control are demonstrated to be able to charge up the DC-side voltage from a 120 V_{AC} RMS supply.

VI. Acknowledgement

This material is based upon work supported by the National Science Foundation Graduate Research Fellowship Program under Grant No. DGE 1752814. Any opinions, findings, and conclusions or recommendations expressed in this material are those of the author(s) and do not necessarily reflect the views of the National Science Foundation.

The information, data, or work presented herein was funded in part by the Advanced Research Projects Agency-Energy (ARPA-E), U.S. Department of Energy, under Award Number DE-AR0000900 in the CIRCUITS program monitored by Dr. Isik Kizilyalli. The views and opinions of authors expressed herein do not necessarily state or reflect those of the United States Government or any agency thereof.

REFERENCES

[1] *SAE Electric Vehicle and Plug in Hybrid Electric Vehicle Conductive Charge Coupler*, 2010. [Online]. Available: https://doi.org/10.4271/J1772_201001

[2] P. K.-H. Dost, P. Spichartz, and C. Sourkounis, "Charging behavior of users utilizing battery electric vehicles and extended range electric vehicles within the scope of a field test," *IEEE Transactions on Industry Applications*, vol. 54, no. 1, pp. 580–590, 2018.

[3] S. Habib, M. M. Khan, K. Hashmi, M. Ali, and H. Tang, "A comparative study of electric vehicles concerning charging infrastructure and power levels," in *2017 International Conference on Frontiers of Information Technology (FIT)*, 2017, pp. 327–332.

[4] Y. Lei, C. Barth, S. Qin, W. C. Liu, I. Moon, A. Stillwell, D. Chou, T. Foulkes, Z. Ye, Z. Liao, and R. Pilawa-Podgurski, "A 2 kW, single-phase, 7-level flying capacitor multilevel inverter with an active energy buffer," *IEEE Transactions on Power Electronics*, vol. 32, no. 11, pp. 8570–8581, Nov 2017. [Online]. Available: http://ieeexplore.ieee.org/stamp/stamp.jsp?arnumber=7811253

[5] D. Chou, Z. Liao, K. Fernandez, T. Gebrael, G. Popovic, R. Mahony, N. Miljkovic, and R. C. N. Pilawa-Podgurski, "An interleaved 6-level gan bidirectional converter with an active energy buffer for level ii electric vehicle charging," in *2021 IEEE Applied Power Electronics Conference and Exposition (APEC)*, 2021, pp. 1203–1208.

[6] Z. Liao, D. Chou, K. Fernandez, Y.-L. Syu, and R. C. Pilawa-Podgurski, "Architecture and control of an interleaved 6-level bidirectional converter with an active energy buffer for level-ii electric vehicle charging," in *2020 IEEE Energy Conversion Congress and Exposition (ECCE)*, 2020, pp. 4137–4142.

[7] Z. Liao, N. C. Brooks, Z. Ye, and R. C. N. Pilawa-Podgurski, "A High Power Density Power Factor Correction Converter with a Multilevel Boost Front-End and a Series-Stacked Energy Decoupling Buffer," in *2018 IEEE Energy Conversion Congress and Exposition (ECCE)*, Sep. 2018, pp. 7229–7235.

[8] S. Coday, N. Ellis, Z. Liao, and R. C. Pilawa-Podgurski, "A lightweight multilevel power converter for electric aircraft drivetrain," in *2021 IEEE Energy Conversion Congress and Exposition (ECCE)*, 2021, pp. 1507–1513.

[9] N. Pallo, S. Coday, J. Schaadt, P. Assem, and R. C. N. Pilawa-Podgurski, "A 10-level flying capacitor multi-level dual-interleaved power module for scalable and power-dense electric drives," in *2020 IEEE Applied Power Electronics Conference and Exposition (APEC)*, 2020, pp. 893–898.

[10] Z. Ye, Y. Lei, Z. Liao, and R. C. N. Pilawa-Podgurski, "Investigation of capacitor voltage balancing in practical implementations of flying capacitor multilevel converters," *IEEE Transactions on Power Electronics*, pp. 1–1, 2021.

[11] D. Reusch and J. Strydom, "Understanding the effect of pcb layout on circuit performance in a high-frequency gallium-nitride-based point of load converter," *IEEE Transactions on Power Electronics*, vol. 29, no. 4, pp. 2008–2015, 2014.

[12] L. Horowitz, N. Pallo, S. Coday, and R. C. Pilawa-Podgurski, "A method of partial inductances to evaluate and optimize switching cells," in *2021 IEEE Applied Power Electronics Conference and Exposition (APEC)*, 2021, pp. 1549–1554.